JBC RESEARCH ARTICLE

Single-molecule fluorescence-based approach reveals novel mechanistic insights into human small heat shock protein chaperone function

Received for publication, July 27, 2020, and in revised form, November 30, 2020 Published, Papers in Press, December 7, 2020,
https://doi.org/10.1074/jbc.RA120.015419

Caitlin L. Johnston[1,2], Nicholas R. Marzano[1,2], Bishnu P. Paudel[1,2], George Wright[3], Justin L. P. Benesch[3], Antoine M. van Oijen[1,2,*], and Heath Ecroyd[1,2,*]

From the [1]Molecular Horizons and School of Chemistry and Molecular Bioscience, University of Wollongong, Wollongong, New South Wales, Australia; [2]Illawarra Health & Medical Research Institute, Wollongong, New South Wales, Australia; and [3]Department of Chemistry, Physical and Theoretical Chemistry, University of Oxford, Oxford, UK

Edited by Ursula Jakob

Small heat shock proteins (sHsps) are a family of ubiquitous intracellular molecular chaperones; some sHsp family members are upregulated under stress conditions and play a vital role in protein homeostasis (proteostasis). It is commonly accepted that these chaperones work by trapping misfolded proteins to prevent their aggregation; however, fundamental questions regarding the molecular mechanism by which sHsps interact with misfolded proteins remain unanswered. The dynamic and polydisperse nature of sHsp oligomers has made studying them challenging using traditional biochemical approaches. Therefore, we have utilized a single-molecule fluorescence-based approach to observe the chaperone action of human alphaB-crystallin (αBc, HSPB5). Using this approach we have, for the first time, determined the stoichiometries of complexes formed between αBc and a model client protein, chloride intracellular channel 1. By examining the dispersity and stoichiometries of these complexes over time, and in response to different concentrations of αBc, we have uncovered unique and important insights into a two-step mechanism by which αBc interacts with misfolded client proteins to prevent their aggregation.

Small heat shock proteins (sHsps) are a diverse and ubiquitously expressed family of intracellular molecular chaperones that play a critical role in the maintenance of protein homeostasis (proteostasis). One of the main roles of sHsps is to bind and trap misfolded proteins to protect cells from irreversible protein aggregation during periods of cellular stress (1–3). Consequently, sHsp malfunction has been implicated in a number of diseases including cataracts, cancer, motor neuropathies, and neurodegeneration (4–6).

Typically sHsps form oligomeric species in solution, and this is thought to be linked to their chaperone function. For example, human alphaB-crystallin (αBc: HSPB5), an archetypal sHsp and one of the most widely expressed of the 10 human sHsp isoforms, forms large, polydisperse oligomeric ensembles in dynamic equilibrium mediated by subunit exchange (7–9). These large oligomers are formed from monomeric and/or dimeric building blocks. Many factors, including the presence of client proteins, temperature, and post-translational modifications, shift the equilibrium from larger polydisperse oligomers to predominantly smaller oligomers, which have been reported to have enhanced chaperone activity (10–15).

It is well established that sHsps can form complexes with misfolded clients to prevent their aggregation (16–18). Studies of monodisperse sHsps from plants, using techniques that include size exclusion chromatography, electron microscopy, and native mass spectrometry, have provided important stoichiometric and mechanistic information on the end-stage complexes that these sHsps form with client proteins (19–24). However, very little is known about the complexes formed between polydisperse mammalian sHsp isoforms and their clients. It has been postulated that for polydisperse sHsps, the initial encounter with client proteins is mediated by smaller sHsp oligomers, which have enhanced chaperone activity as a result of increased exposed hydrophobicity and, therefore, a greater affinity for misfolded and aggregation-prone proteins (25–28). Nevertheless, the initial encounter of an sHsp with an aggregation-prone client protein has never been observed. Thus, it remains unclear precisely how sHsps capture misfolded proteins to form the sHsp–client complexes observed as a result of their chaperone action.

Single-molecule fluorescence techniques overcome some of the difficulties of studying dynamic and heterogeneous systems by facilitating the observation of individual protein–protein interactions. Consequently, such approaches may be advantageous for the study of molecular chaperones (29, 30) since, in the case of sHsps, they may enable the intial steps of binding with client proteins to be observed and therefore the molecular mechanism of chaperone action of sHsps to be revealed. Thus, in this work we have exploited a single-molecule fluoresence-based assay in order to directly observe complexes formed between αBc and a model client protein, the chloride intracellular channel 1 (CLIC1) protein.

* For correspondence: Antoine M. van Oijen, vanoijen@uow.edu.au; Heath Ecroyd, heathe@uow.edu.au.

We demonstrate that αBc inhibits the heat-induced amorphous aggregation of CLIC1 and that this inhibitory activity results in the formation of a polydisperse range of αBc–CLIC1 complexes. Employing our single-molecule fluorescence-based assay, we have, for the first time, determined the stoichiometries of complexes formed between αBc and a client protein and measured how these complexes change over time. Our results provide evidence for a two-step mechanism of sHsp–client interaction and provide fundamental insight into the molecular mechanisms by which sHsps interact with client proteins to prevent aggregation as part of proteostasis.

Results

CLIC1—a new model client protein for assessing sHsp chaperone activity

CLIC proteins can exist in cells in both a soluble globular form as well as an integral membrane protein with ion channel function (31). The soluble globular form of CLIC1 adopts a glutathione-S-transferase (GST)–like canonical fold and is monomeric (31–33). We chose to explore CLIC1 as a potential model client protein to study sHsp chaperone function because cytosolic plant sHsps have been shown to bind GST proteins *in vivo* following heat stress (34) and expression of the human sHsp, Hsp27 (HSPB1) protects detoxifying enzymes, such as GSTs, against inactivation in cells (35). Destabilization of CLIC1, whether through a change in pH or temperature, results in the formation of a folding intermediate with a high degree of solvent-exposed hydrophobicity (36, 37), causing it to be decidedly aggregation-prone. This is typical of the client proteins of sHsps that form during times of cellular stress, whereby sHsps bind to these destabilized forms to prevent their aggregation (38). Isoforms of CLIC1 amenable to site-specific labeling at cysteine residues have been previously described (39), including an isoform in which four of the six native cysteines are mutated to alanines (C89A, C178A, C191A, C223A; herein designated $CLIC1_{cysL}$). Together, these characteristics led us to develop CLIC1 as a model client protein for the study of αBc chaperone activity at the single-molecule level.

We first confirmed that heat destabilization of $CLIC1_{cysL}$ led to its aggregation, akin to the behavior of other client proteins, including luciferase, rhodanese, alcohol dehydrogenase, and malate dehydrogenase, which are typically used to assess chaperone function (40, 41). When $CLIC1_{cysL}$ was incubated at 37 °C, there was a significant increase in light scattering at 340 nm over 20 h, indicative of its destabilization and subsequent aggregation (Fig. 1*A*). However, when $CLIC1_{cysL}$ was incubated in the presence of αBc_{WT}, there was a concentration-dependent reduction in the rate and overall amount of light scatter associated with $CLIC1_{cysL}$ aggregation (Fig. 1, *A*–*B*). The specificity of this effect was demonstrated by a negative control (using the non-chaperone protein ovalbumin) not inhibiting the increase in light scatter associated with the aggregation of $CLIC1_{cysL}$. Furthermore, there was no increase in light scatter when αBc_{WT} was incubated alone, demonstrating that the increase in light scatter was exclusively due to the aggregation of $CLIC1_{cysL}$. Analysis by size exclusion chromatography and SDS-PAGE of samples following incubation showed that, when incubated together at a molar ratio of 1:0.5 (αBc_{WT}:$CLIC1_{cysL}$), αBc_{WT} and $CLIC1_{cysL}$ coeluted in early fractions (fractions 7–9) from the column, suggesting that αBc_{WT} prevented the heat-induced aggregation of $CLIC1_{cysL}$ *via* the formation of high-molecular mass complexes (Fig. 1, *C*–*D*, Fig. S1). Thus, mild heating at 37 °C leads to the destabilization and aggregation of CLIC1, and αBc_{WT} can inhibit this process by forming complexes with the aggregation-prone protein, demonstrating the utility of CLIC1 as a good model client protein for monitoring molecular chaperone activity.

Examining the interaction of αBc with CLIC1 via *single-molecule FRET*

To further characterize the nature of the physical interaction between CLIC1 and αBc, we utilized a single-molecule FRET (smFRET)–based approach that allows interactions between biomolecules to be observed (at separations of 2–10 nm). For these experiments, we generated $CLIC1_{C24}$, a CLIC1 isoform that contains a mutation of one of the native tryptophan residues to phenylalanine (W23F) and mutations of five of the native cysteines to alanines (C59A, C89A, C178A, C191A, and C223A); the remaining cysteine (C24) was not modified so it could be exploited for site-specific fluorescent labeling. As observed for $CLIC1_{cysL}$, incubation of $CLIC1_{C24}$ at 37 °C resulted in a significant increase in light scattering at 340 nm over 20 h, indicative of its aggregation, and this was inhibited in a concentration-dependent manner by αBc_{WT}, but not the non-chaperone control proteins superoxide dismutase 1 (SOD1: Fig. 2, *A*–*B*) or ovalbumin (Fig. S2*C*). Interestingly, cross-linking of αBc_{WT} had no significant impact on its capacity to inhibit the aggregation of $CLIC1_{C24}$ (Fig. S2, *D*–*F*), suggesting that dynamic subunit exchange of αBc oligomers is not required for the chaperone action in this assay.

To perform smFRET on complexes formed between CLIC1 and αBc, we site-specifically labeled $CLIC1_{C24}$ with an Alexa Flour 555 donor fluorophore. A mutant of αBc (αBc_{C176}) was used in these experiments that contains an additional cysteine at the extreme C-terminus of the protein for site-specific attachment of an Alexa Fluor 647 acceptor fluorophore. The addition of the C-terminal cysteine did not affect the ability of the chaperone to inhibit $CLIC1_{C24}$ aggregation (Fig. S2*A*) or substantially change the oligomeric distribution of the protein according to mass photometry measurements (Fig. S3). Mass photometry measurements revealed that while the addition of the fluorescent dye to the C-terminal cysteine did cause a shift in the oligomeric distribution of αBc_{C176} toward smaller species, the protein was still capable of forming larger oligomers. To determine if the fluorescently labeled αBc_{C176} could interact and form client–chaperone complexes with $CLIC1_{C24}$, donor (AF555)-labeled $CLIC1_{C24}$ and acceptor (AF647)-labeled αBc_{C176} were incubated together at 37 °C for 20 h and immobilized on a functionalised coverslip for total internal reflection fluorescence (TIRF) microscopy (Fig. 2*C*). Complexes containing colocalized $CLIC1_{C24}$ and αBc_{C176} were

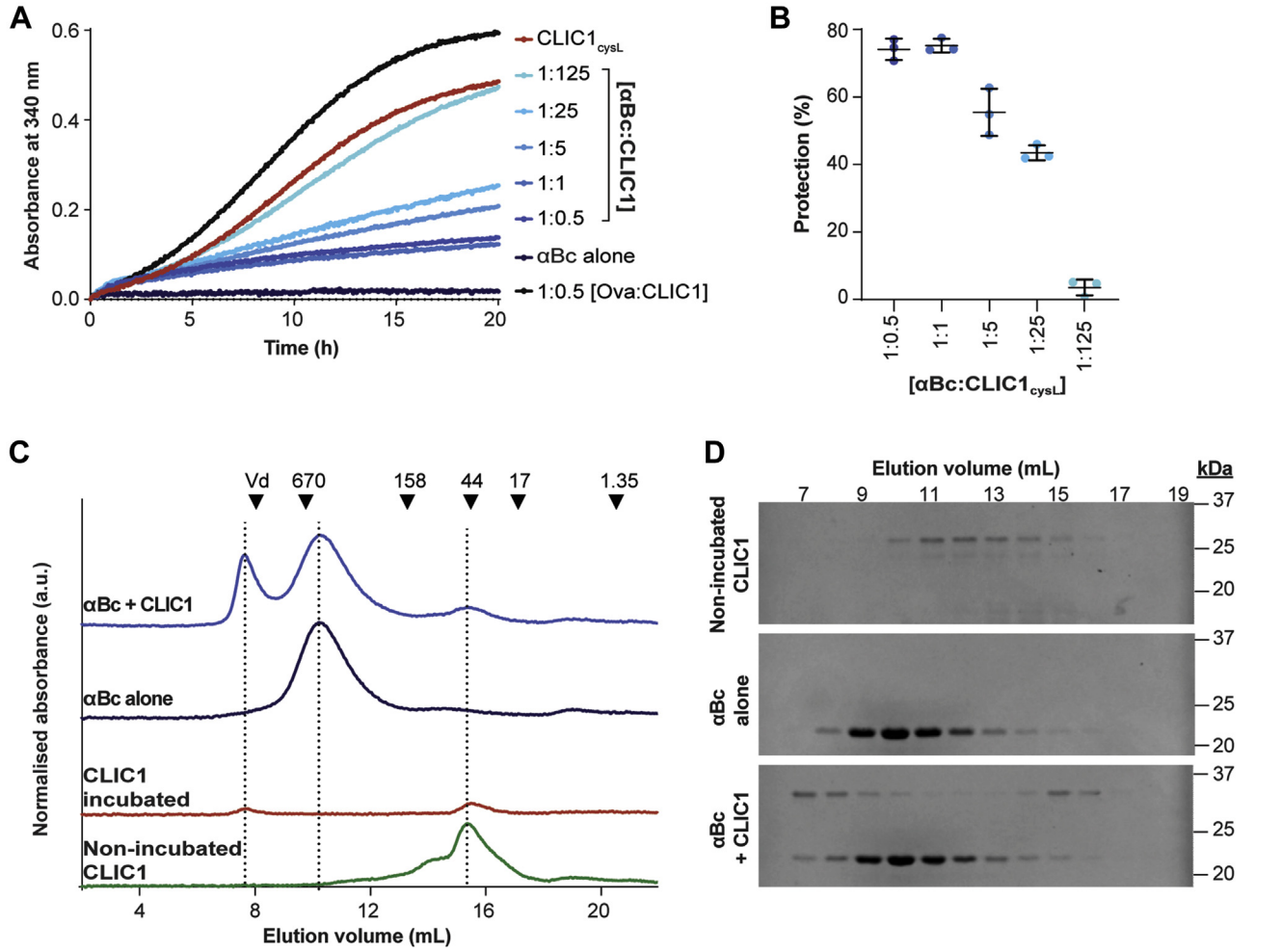

Figure 1. αBc_{WT} forms high-molecular-mass complexes with $CLIC1_{cysL}$, inhibiting its amorphous aggregation. *A*, $CLIC1_{cysL}$ (50 μM) was incubated at 37 °C for 20 h in the presence of varying molar ratios of αBc_{WT} (1:125–1:0.5, αBc_{WT}–CLIC1) or ovalbumin (Ova). Ovalbumin was used as a non-chaperone control protein at a molar ratio of 1:0.5 (CLIC1–Ova). The aggregation of $CLIC1_{cysL}$ was monitored by measuring the change in light scatter at 340 nm over time. *B*, the percentage protection afforded by varying molar ratios of αBc_{WT} against $CLIC1_{cysL}$ aggregation, reported as the mean ± standard deviation of three independent experiments (n = 3). *C*, size-exclusion chromatograms of non-incubated $CLIC1_{cysL}$ (50 μM) (*green*), and the soluble fraction of samples following incubation; $CLIC1_{cysL}$ in the absence of αBc_{WT} (*red*); αBc_{WT} alone (100 μM, *dark blue*); $CLIC1_{cysL}$ in the of presence αBc_{WT} (*light blue*, molar ratio 1:0.5, αBc_{WT}:CLIC1). *D*, SDS-PAGE of the eluted fractions collected from the size-exclusion column. The elution volume of the fractions is shown at the top of the figure.

observed at the single-molecule level (Fig. 2*D*), and the approximate time–FRET traces were calculated using the donor and acceptor fluorescence time–intensity traces (Fig. S4*A*). The time-FRET trajectories initially displayed high FRET efficiencies, which gradually decreased over time, likely due to the photobleaching of multiple acceptor fluorophores within the αBc_{C176}–$CLIC1_{C24}$ complexes (Fig. S4*B*). Analysis of the initial FRET efficiency of αBc_{C176}–$CLIC1_{C24}$ complexes prior to photobleaching showed these complexes had a high FRET efficiency (E = 0.8–1) and therefore were in close proximity, consistent with a stable interaction between αBc_{C176} and heat-destabilized $CLIC1_{C24}$ (Fig. 2*E*). However, the complexity of these smFRET traces, as a result of multiple donor and acceptor fluorophores within the complexes, means calculation of accurate distances between acceptor and donor fluorophores and the precise stoichiometries of αBc_{C176} and $CLIC1_{C24}$ cannot readily be determined using this approach.

A single-molecule fluorescence-based approach can be used to examine interactions between αBc and CLIC1

We hence sought to employ a single-molecule fluorescence-based assay that would enable the stoichiometries of αBc_{C176} and $CLIC1_{C24}$ within complexes to be interrogated. To do so, we first investigated the binding of heated (37 °C for 2 h) site-specific fluorescently labeled $CLIC1_{C24}$ (AF647-$CLIC1_{C24}$) to the surface of a functionalised coverslip (Fig. 3*A*). As expected, there was a significant increase in the number of $CLIC1_{C24}$ foci observed when the capture antibody was present (Fig. 3*B*). Moreover, there was no difference in the fluorescent intensities of the $CLIC1_{C24}$ species bound to the coverslip in the presence or absence of the antibody (Fig. 3*C*), demonstrating that the $CLIC1_{C24}$ bound by the antibody is representative of the $CLIC1_{C24}$ species present in solution. Heated $CLIC1_{C24}$ was immobilized to the functionalized coverslip much more readily than folded $CLIC1_{C24}$ (Fig. 3, *D*–*F*), presumably due to increased exposure of the N-terminal His-tag as a result of

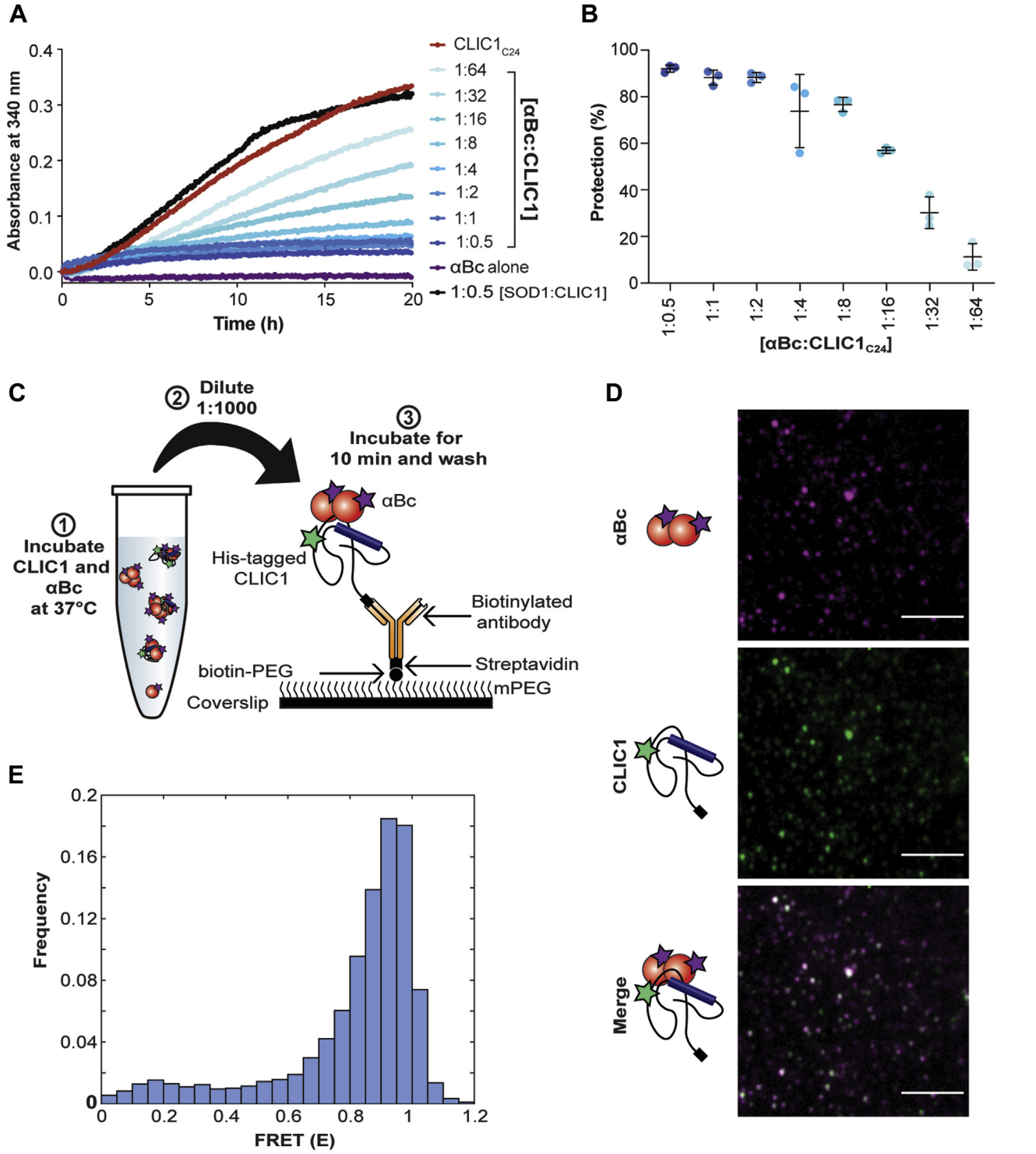

Figure 2. αBc binds and inhibits the amorphous aggregation of CLIC1$_{C24}$ by forming stable client–chaperone complexes. *A*, a representative aggregation assay performed to assess the ability of αBc$_{WT}$ to inhibit the heat-induced aggregation of CLIC1$_{C24}$. Recombinant CLIC1$_{C24}$ was incubated at 37 °C for 20 h in the presence or absence of varying molar ratios of αBc$_{WT}$ (1:0.5–1:64, αBc$_{WT}$–CLIC1$_{C24}$) or the control protein SOD1. The aggregation of CLIC1$_{C24}$ was monitored by measuring the change in light scatter at 340 nm over time. *B*, the percent inhibition afforded by varying molar ratios of αBc$_{WT}$ against CLIC1$_{C24}$ aggregation, reported as mean ± standard deviation of three independent aggregation assays (n = 3). *C*, schematic of methodology used to form and surface immobilize complexes formed between AF555-CLIC1$_{C24}$ and AF647-αBc$_{C176}$ for smFRET experiments. *D*, representative TIRF microscopy images of AF555-CLIC1$_{C24}$ and AF647-αBc$_{C176}$ complexes. *Scale bar* = 5 μm. *E*, FRET efficiency *(E)* histogram derived from TIRF microscopy data of the initial intensities of CLIC1$_{C24}$–αBc$_{C176}$ complexes prior to photobleaching (n = 421 molecules). αBc, alphaB-crystallin; SOD1, superoxide dismutase 1; TIRF, total internal reflection fluorescence.

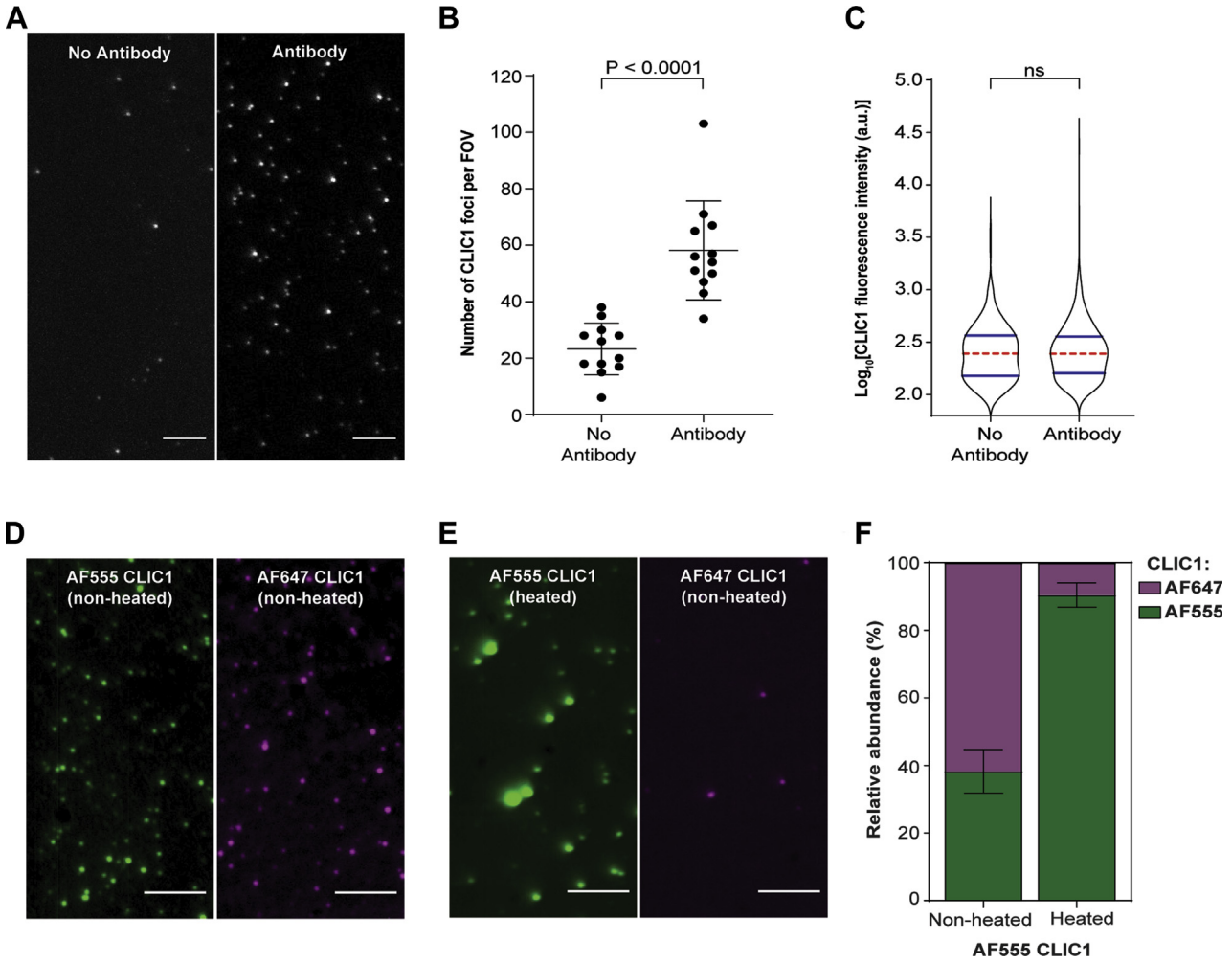

Figure 3. The binding of CLIC1 to functionalized coverslips for analysis by a single-molecule fluorescence-based approach. *A–C*, AF647-labeled $CLIC1_{C24}$ (1 μM) was incubated at 37 °C for 2 h before being diluted 1:1000 into imaging buffer and loaded into flow cells in the presence and absence of a surface-bound anti-6X His-tag antibody. Following a 10-min incubation, flow cells were washed and imaged using TIRF microscopy. *A*, representative images of surface-bound AF647-$CLIC_{C24}$ in the absence (*left*) or presence (*right*) of surface-immobilized antibodies. *Scale bar* = 5 μm. *B*, the number of $CLIC1_{C24}$ foci per field of view (FOV) on coverslips in the presence or absence of the anti-6X His-tag antibody, reported as mean ± standard deviation (n = 12). Comparisons of the treatment groups were performed *via* a student's *t* test. *C*, violin plots showing the distribution of the fluorescence intensity of AF647-$CLIC1_{C24}$ foci in the presence or absence of the antibody. The plots show the kernel probability density (*black outline*), median (*red*), and interquartile range (*blue*). Comparisons of distributions were performed using the Kruskal–Wallis test for multiple comparisons with Dunn's procedure. *D–F*, AF647-$CLIC1_{C24}$ was incubated in the presence of heated (previously for 2 h at 37 °C) or nonheated AF555-$CLIC1_{C24}$ (1 μM) for 5 min on ice. Samples were diluted 1:1000 and were loaded into flow cells before being washed and imaged using TIRF microscopy. Representative images of surface-bound (*D*) nonheated AF555-$CLIC1_{C24}$ (*green*) and AF647-$CLIC1_{C24}$ (*magenta*) or (*E*) heated AF555-$CLIC1_{C24}$ (*green*) and nonheated AF647-$CLIC1_{C24}$ (*magenta*). *F*, the relative abundance of each fluorescently labeled $CLIC1_{C24}$ species per FOV reported as mean ± standard deviation (n = 15). TIRF, total internal reflection fluorescence.

$CLIC1_{C24}$ unfolding. Thus, our single-molecule approach efficiently captures the thermally destabilized $CLIC1_{C24}$ species that are potential clients of sHsps.

We next incubated AF647-$CLIC1_{C24}$ and AF488-αBc_{C176} together at 37 °C and collected aliquots at various timepoints over a 10-h period. Samples were then diluted and immediately immobilized to the coverslip surface (*via* the His-tag on $CLIC1_{C24}$) for imaging using TIRF microscopy. As expected, αBc_{C176} (green) was observed to colocalize with $CLIC1_{C24}$ molecules (magenta) (Fig. 4*A*), indicative of the formation of stable complexes between these two proteins and consistent with the results of the smFRET experiments (Fig. 2*D*). The proportion of $CLIC1_{C24}$ molecules colocalized with αBc_{C176} increased rapidly over 1 h (Fig. 4*B*). Interestingly, after 4 h, the proportion of $CLIC1_{C24}$ colocalized with αBc_{C176} reached a maximum of approximately 50%, demonstrating that not all $CLIC1_{C24}$ molecules were in complex with αBc_{C176} under these experimental conditions (these $CLIC1_{C24}$ molecules not in complex with αBc_{C176} are herein referred to as free $CLIC1_{C24}$ species). Additionally, despite having blocked (passivated) the coverslip surface, which significantly reduced the nonspecific binding of αBc_{C176} to the coverslip, some nonspecific binding of αBc_{C176} molecules not in complex with $CLIC1_{C24}$ was also observed (herein referred to as free αBc_{C176} species) (Fig. 4*A*). Negative stain transmission electron microscopy (TEM) demonstrated the heterogeneous nature of the AF488-αBc_{C176} oligomers and the species present following incubation of AF647-$CLIC1_{C24}$ and AF488-αBc_{C176}

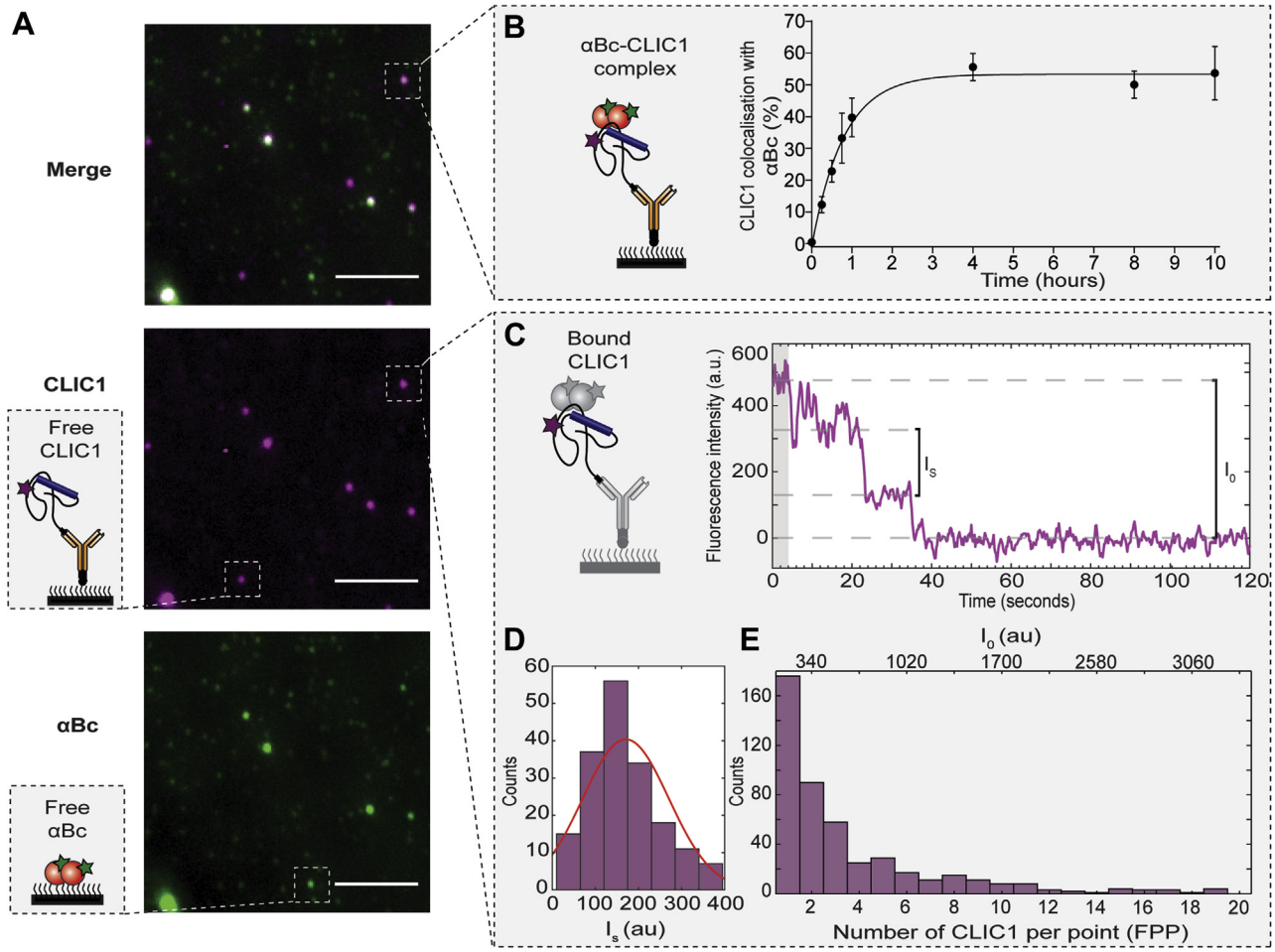

Figure 4. Characterization of $CLIC1_{C24}$–αBc_{C176} complexes using a single-molecule fluorescence-based approach. AF488-αBc_{C176} was incubated with AF647-$CLIC1_{C24}$ (2:1 molar ratio) at 37 °C for 10 h to form complexes. Aliquots were taken at multiple timepoints throughout the incubation for TIRF microscopy imaging. *A*, representative TIRF microscopy images of complexes at 10 h. *Scale bar* = 5 μm. Schematic indicating free $CLIC1_{C24}$ and αBc_{C176} bound to the coverslip surface. *B*, schematic showing the immobilization of αBc_{C176}–$CLIC1_{C24}$ complexes to the surface of a glass coverslip. The percentage of $CLIC1_{C24}$ colocalized with αBc_{C176} over time reported as the mean ± standard deviation of three independent experiments. Data were fit using a one-phase association model. *C*, example time trace of the fluorescent intensity of AF647-$CLIC1_{C24}$ in complex with AF488-αBc_{C176}. The shaded area (*gray*) represents the first 20 values that were averaged to determine the initial intensity (I_0). *D*, photobleaching traces from AF647-$CLIC1_{C24}$ molecules with distinct photobleaching steps were manually identified and fit to a change point analysis to calculate the fluorescent intensity of each single-photobleaching event (I_s). The I_s values were fit to a Gaussian distribution to determine the mean intensity of a single photobleaching event ($I_{s\text{-}mean}$). *E*, example histogram of $CLIC1_{C24}$ showing the distribution of I_0 and fluorescently labeled proteins per point (FPP) at 10 h. FPP were calculated using the equation $FPP = I_0/I_{s\text{-}mean}$ for all the $CLIC1_{C24}$ in complex with αBc_{C176}. TIRF, total internal reflection fluorescence.

at 37 °C (Fig. S5). This heterogeneity precluded any detailed analysis of complexes formed between $CLIC1_{C24}$ and αBc_{C176} *via* TEM; however, we did observe an apparent reduction in the size of species in samples containing both $CLIC1_{C24}$ and αBc_{C176} compared with those containing only αBc_{C176}.

To determine the stoichiometries of $CLIC1_{C24}$ and αBc_{C176} in complexes formed under conditions in which $CLIC1_{C24}$ is prone to aggregation, molecules were imaged until all fluorophores were completely photobleached. $CLIC1_{C24}$ and αBc_{C176} trajectories with distinct photobleaching steps were identified manually and used to calculate the fluorescent intensity of each single-photobleaching event (I_s) (Fig. 4*C*, Figs. S6, *A* and *D* and S7*B*). The I_s values collected from $CLIC1_{C24}$ and αBc_{C176} trajectories containing one distinct photobleaching step were not significantly different when the proteins were in a complex or alone (αBc_{C176} nonspecifically bound to the surface was used to assess the protein when not in a complex) (Fig. S6, *B* and *E*). Therefore, binding of the two proteins into a complex did not significantly affect the fluorescent intensity of the fluorophores attached to the proteins. Analysis of trajectories from $CLIC1_{C24}$–αBc_{C176} complexes that contained multiple distinct photobleaching steps showed a broader distribution of I_S values than complexes containing only a single unit of either protein (Fig. S6, *B* and *E*). Thus, to establish the number of $CLIC1_{C24}$ or αBc_{C176} in complexes, I_s values calculated from trajectories with multiple distinct photobleaching steps were fit to a Gaussian distribution from which the mean intensity of a single photobleaching event ($I_{s\text{-}mean}$) for $CLIC1_{C24}$ or αBc_{C176} was derived (Fig. 4*D*, Fig. S7*C*). The $I_{s\text{-}mean}$ values determined using change point analysis were 170.5 ± 99 a.u and 166 ± 119 a.u for $CLIC1_{C24}$ and αBc_{C176}, respectively. These values were then used to determine the number of fluorescently labeled proteins per point (*FPP*). The initial fluorescence intensities (I_0) for $CLIC1_{C24}$ and

αBc_{C176} in each complex were calculated by averaging the first 20 intensity values (Fig. 4*C*, Fig. S7*B*). Change point analysis was not used to calculate I_0 owing to its inability to accurately fit photobleaching steps of larger complexes (*i.e.*, >10mers). Furthermore, calculation of I_0 *via* either change point analysis or averaging of the initial 20 intensity values of trajectories yielded similar values when used to analyze $CLIC1_{C24}$ and αBc_{C176} trajectories (<10mers) with multiple distinct photobleaching steps (Fig. S6, *C* and *F*). Subsequently I_0 for $CLIC1_{C24}$ and αBc_{C176} in each complex was divided by the appropriate $I_{s\text{-}mean}$ to calculate the *FPP*. These *FPP* values were then used to determine the number of subunits of each protein present in complexes of up to a maximum of 20 subunits (Fig. 4*E*, Fig. S7*D*; see Two-color TIRF microscopy data and statistical analysis in the Experimental procedures section).

To investigate whether the dilution and immobilization of αBc_{C176}–$CLIC1_{C24}$ complexes required for this single-molecule fluorescence approach affected the nature of the complexes formed at higher concentrations, complexes were cross-linked prior to dilution and single-molecule measurements (Fig. S8). When αBc_{C176} was cross-linked in the absence of $CLIC1_{C24}$ and diluted for TIRF microscopy, a small decrease in the αBc_{C176} oligomer size indicative of some dissociation of large oligomers was observed (Fig. S8, *A*–*C*). However, this decrease in the size of αBc_{C176} oligomers was not observed when it was in complex with $CLIC1_{C24}$ (Fig. S8, *E*, *G* and *H*). Furthermore, the size and amount of $CLIC1_{C24}$ in complex with αBc_{C176} was not significantly affected by dilution and immobilization of the complexes (Fig. S8, *E*, *G* and *H*), indicating that the complexes observed by single-molecule fluorescence imaging are representative of those formed during the incubation at 37 °C. However, when comparing the size distributions of αBc_{C176} observed by this single-molecule fluorescence approach with those obtained by mass photometry, it is apparent that the single-molecule fluorescence approach primarily detects the smaller oligomers (<10 subunits) (Fig. S8*D*).

The size and polydispersity of complexes formed between αBc and CLIC1 increase over time

To obtain further information on the interaction between αBc_{C176} and $CLIC1_{C24}$, we examined the change in size and composition of the αBc_{C176}–$CLIC1_{C24}$ complexes over time, as well as the size of the molecules that were not in complex. Prior to incubation, both $CLIC1_{C24}$ and αBc_{C176} were present predominantly as smaller noncolocalized species (Fig. 5, *A* and *E*). Following incubation at 37 °C for 0.25 h, αBc_{C176} was found bound to oligomeric species of $CLIC1_{C24}$ that were significantly larger in size than free $CLIC1_{C24}$ species (Fig. 5*B*, $p < 0.0001$). After 0.25 h of incubation, both the bound and free $CLIC1_{C24}$ oligomers did not increase in size (Fig. 5, *A* and *C*). Moreover, the $CLIC1_{C24}$ species not in complex were significantly smaller than the bound species throughout the entire incubation period (Fig 5*D*). Interestingly, following incubation, the size of the noncomplexed $CLIC1_{C24}$ significantly decreased ($p < 0.001$), such that by 10 h primarily monomers were present. This suggests that $CLIC1_{C24}$ species larger than monomers were preferentially bound by αBc_{C176} upon heating.

During the early stages of the incubation (up to 0.5 h), αBc_{C176} in complex with $CLIC1_{C24}$ was primarily monomeric or dimeric (Fig. 5*E*). However, after 0.5 h of incubation, the number of αBc_{C176} molecules in these complexes significantly increased over time, reaching a maximum after 1 h. Analysis of nonspecifically adsorbed αBc_{C176} species indicated that they were significantly smaller in size than αBc_{C176} that was in complex with $CLIC1_{C24}$ throughout the incubation period ($p < 0.0001$; Fig. 5*F*, Fig. S9).

We next utilized our single-molecule fluorescence-based approach to characterize the stoichiometries of αBc_{C176}–$CLIC1_{C24}$ in individual complexes and interrogate how these change as a function of incubation time. For each individually identified αBc_{C176}–$CLIC1_{C24}$ complex, we determined the αBc_{C176}–$CLIC1_{C24}$ stoichiometry by calculating the number of monomers of each protein present. This process allowed us to quantify the relative abundance of these stoichiometries over time. Interestingly, we observed that complexes became increasingly polydisperse over the observation time (Fig. 5*G*). At early timepoints during the incubation (0.25–0.5 h), complexes were comprised predominantly of smaller species of αBc_{C176} (monomers-3mers) bound to a polydisperse range of $CLIC1_{C24}$ oligomers (monomers to 12mers). The most abundant complex observed was comprised of monomeric αBc_{C176} bound to a single subunit of $CLIC1_{C24}$. The polydispersity of $CLIC1_{C24}$ within complexes (monomers to 12mers) did not change greatly over 8 h; however, the relative abundance of complexes with more αBc_{C176} (>6mers) increased after 1 h. This increase in the number of αBc_{C176} monomers present in complexes was consistent with the observed increase in the size distribution of αBc_{C176} over time (Fig. 5*E*). Together, these results suggest smaller αBc_{C176} subunits initially bind to aggregation-prone $CLIC1_{C24}$ to form chaperone–client complexes and, over time, additional free αBc_{C176} subunits bind to these complexes until the system reaches equilibrium.

Chaperone concentration influences the stoichiometries of CLIC1–αBc complexes

The molar ratio of sHsp to client protein is thought to be one of the most important parameters that determines the nature and size of sHsp–client complexes (18-21, 23, 42, 43). Therefore, we exploited our single-molecule fluorescence assay to investigate how sHsp concentration affects the stoichiometries of complexes formed with $CLIC1_{C24}$. We observed that the size of $CLIC1_{C24}$ species in complex with αBc_{C176} significantly increased with increasing relative amounts of αBc_{C176} (molar ratios from 0.25:1 to 4:1, αBc_{C176}–$CLIC1_{C24}$) (Fig. 6*A*). Conversely, the number of αBc_{C176} subunits in complexes was significantly smaller ($p < 0.0001$) when the sHsp was present at a molar ratio below or equal to the amount of $CLIC1_{C24}$ present (0.25:1–1:1, αBc_{C176}–$CLIC1_{C24}$) (Fig. 6*B*). The number of αBc_{C176} subunits in complexes significantly increased when the αBc_{C176} was present in excess of $CLIC1_{C24}$ (2:1 and 4:1, αBc_{C176}–$CLIC1_{C24}$) (Fig. 6*B*). At all molar ratios tested, both αBc_{C176} and $CLIC1_{C24}$ were significantly larger when in complex than when they were not in complex (Fig. S10, *B*–*E*). Interestingly, noncolocalized αBc_{C176}

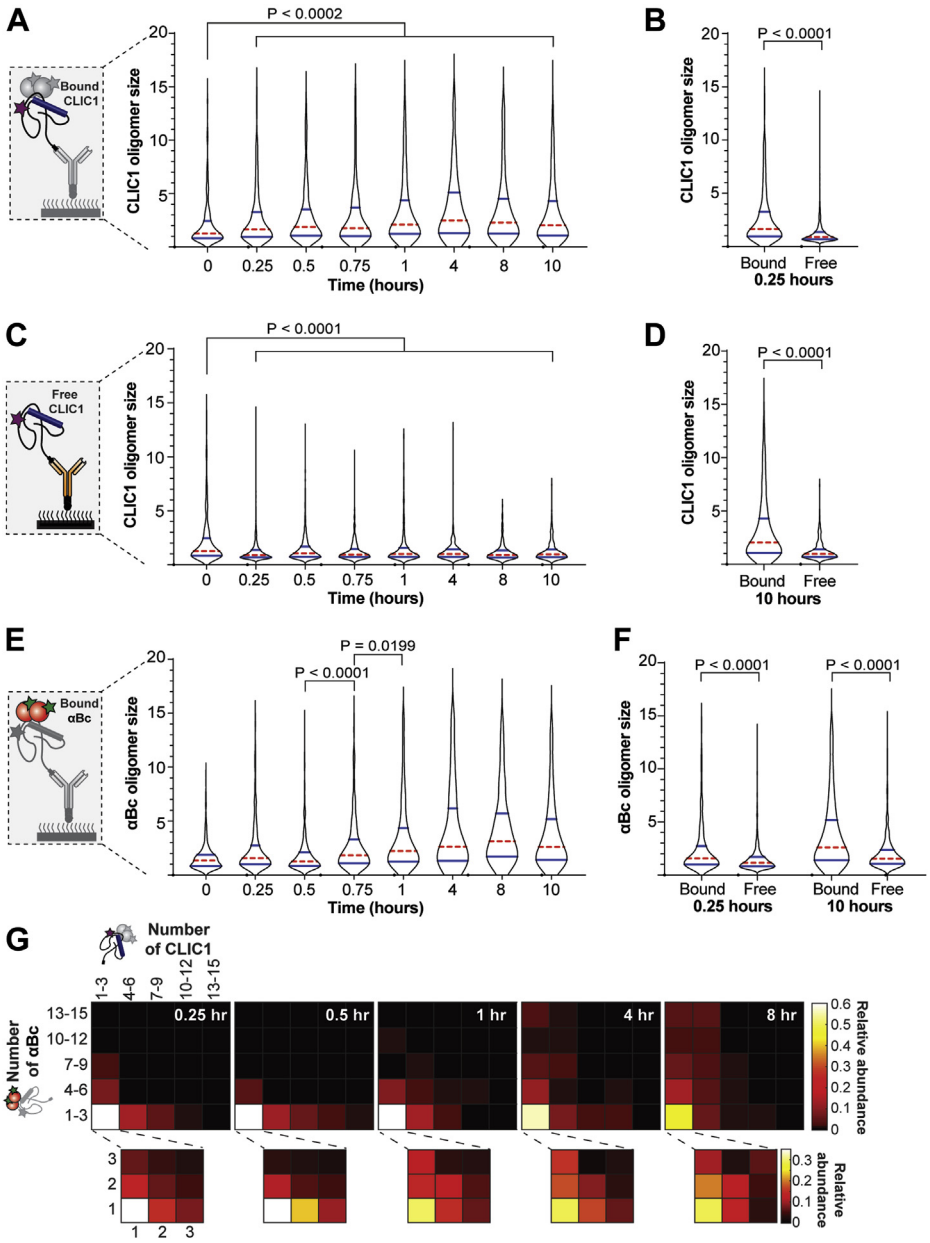

Figure 5. αBc_{C176}-$CLIC1_{C24}$ complexes increase in polydispersity and size over time. AF488-αBc_{C176} was incubated with AF647–$CLIC1_{C24}$ (2:1 molar ratio) at 37 °C for 10 h, with aliquots taken at multiple timepoints throughout the incubation. Following incubation, aliquots were immediately diluted and incubated in flow cells for 10 min before being washed and imaged using TIRF microscopy. Violin plots showing the size distribution over 10 h at 37° of (*A*) free $CLIC1_{C24}$ that is not in complex with αBc_{C176}, (*B*) $CLIC1_{C24}$ bound to αBc_{C176} or free $CLIC1_{C24}$ after 0.25 h of incubation, (*C*) $CLIC1_{C24}$ bound to αBc_{C176}, (*D*) $CLIC1_{C24}$ bound to αBc_{C176} or free $CLIC1_{C24}$ after 10 h of incubation, (*E*) αBc_{C176} bound to $CLIC1_{C24}$, and (*F*) αBc_{C176} bound to $CLIC1_{C24}$ or nonspecifically adsorbed to the surface (Free) after 10 h. The violin plots show the kernel probability density (*black outline*), median (*red*), and interquartile range (*blue*). Results include measurements from three independent experiments (n = 3), and comparisons of distributions were performed using the Kruskal–Wallis test for multiple comparisons with Dunn's procedure (*p* values indicated). *G*, heatmaps showing the relative abundance of αBc_{C176}–$CLIC1_{C24}$ complexes and their stoichiometries over 8 h of incubation. TIRF, total internal reflection fluorescence.

was observed to be significantly larger in size when incubated at the higher concentrations (>1 μM) used in these experiments (Fig. S10*D*).

As observed previously, the complexes formed between αBc_{C176} and $CLIC1_{C24}$ after heating were heterogeneous (Fig. 6*C*). Examination of the relative abundance of complexes formed when the molar ratio of αBc_{C176}–$CLIC1_{C24}$ was low ([0.25:1]–[1:1]) indicated that a small number of αBc_{C176} subunits (monomers-6mers) were in complex with $CLIC1_{C24}$ species (monomers-6mers). In contrast, when complexes were formed at higher molar ratios of αBc_{C176}–$CLIC1_{C24}$ ([2:1]–[4:1]), although the number of $CLIC1_{C24}$ species within the complexes did not change (monomers-6mers), the complexes did increase in the number of αBc_{C176} subunits (>10mers). Consequently, these data suggest that higher concentrations of αBc_{C176} result in an increased binding of free αBc_{C176} subunits to the initial complexes that are formed with $CLIC1_{C24}$.

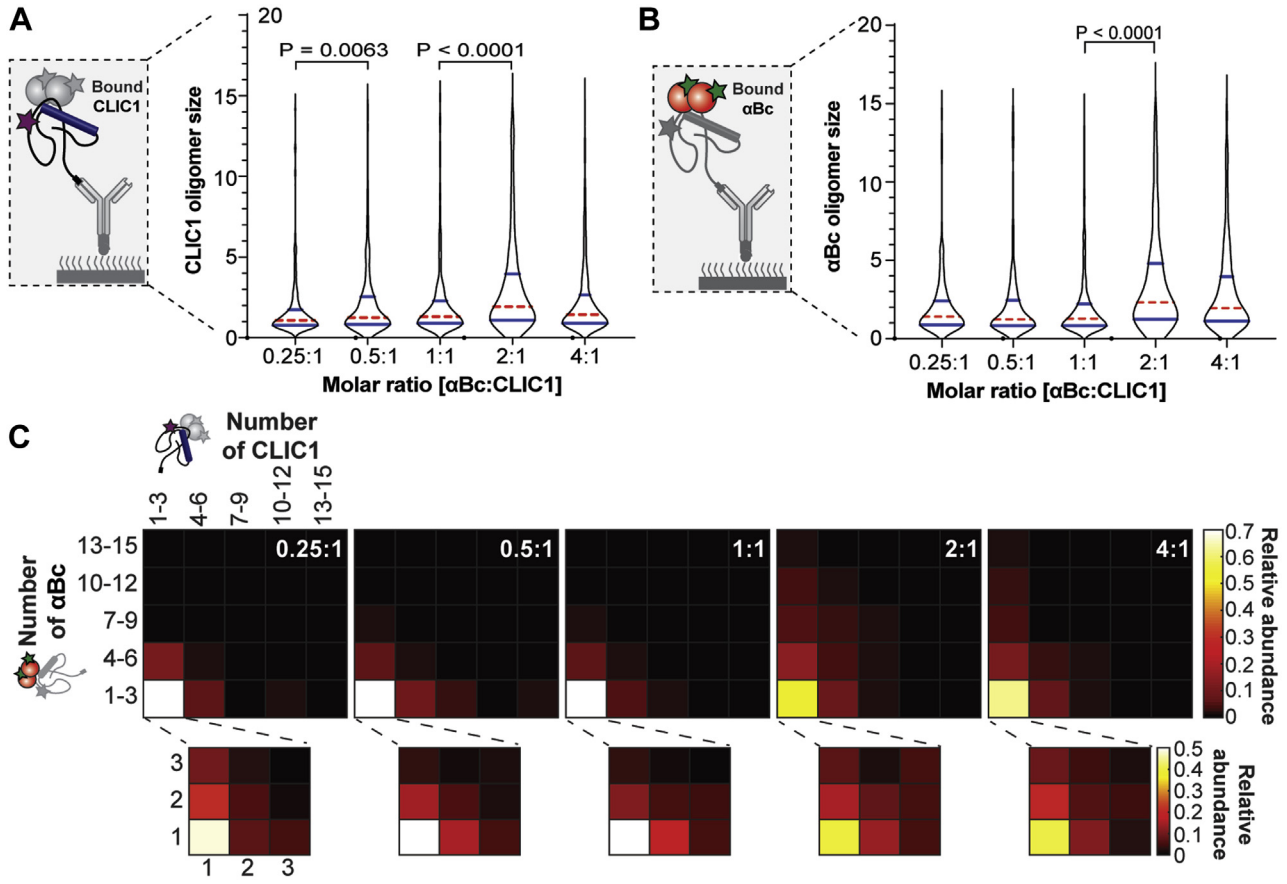

Figure 6. αBc_{C176}–$CLIC1_{C24}$ complexes change in size and stoichiometry with increasing αBc_{C176} concentration. AF647-$CLIC1_{C24}$ was incubated in the presence of varying molar ratios of AF488-αBc_{C176} at 37 °C for 8 h. Following incubation, samples were immediately diluted and incubated in flow cells for 10 min before being washed and imaged using TIRF microscopy. The size distributions of $CLIC1_{C24}$ (*A*) in complex with αBc_{C176} (*B*) at increasing molar ratios of αBc_{C176}–$CLIC1_{C24}$. The violin plots show the kernel probability density (*black outline*), median (*red*), and interquartile range (*blue*). Result are representative of two independent experiments (n = 2), and comparisons of distributions were performed using the Kruskal–Wallis test for multiple comparisons with Dunn's procedure (*p* values indicated). *C*, heatmaps showing the relative abundance of αBc_{C176}–$CLIC1_{C24}$ complexes with increasing molar ratios of αBc_{C176}–$CLIC1_{C24}$. TIRF, total internal reflection fluorescence.

Discussion

In this study, we set out to detect and quantify for the first time the initial binding events between an sHsp and client protein. To do so, we employed single-molecule fluorescence assays to study the chaperone action of αBc, an archetypal mammalian sHsp. By employing this single-molecule fluorescence-based approach, we have determined the stoichiometries of complexes formed between αBc and a client protein, CLIC1. From examination of the polydispersity and stoichiometries of these complexes over time, we have uncovered unique and important insights into the mechanism by which αBc captures misfolded client proteins to prevent their aggregation.

The most commonly used approach to investigate chaperone activity is assays that monitor the aggregation of proteins *in vitro*, *via* either light scatter or, in the case of amyloid fibril formation, fluorescent dyes such as Thioflavin T (44). We exploited CLIC1 as a model client protein in this work since it has been previously shown that sHsps interact with proteins with a GST fold in heat-stressed plants (34) and destabilization of CLIC1 results in it forming a folding intermediate with a high degree of solvent-exposed hydrophobicity (36, 37), which is typical of sHsp client proteins that form during cellular stress. Indeed, we demonstrate *via* a light scattering assay that mild heating at 37 °C leads to the aggregation of the CLIC1 isoforms used in this work. Moreover, αBc is able to effectively inhibit this heat-induced aggregation of CLIC1 by forming complexes with it. However, these bulk ensemble assays struggle to provide mechanistic details concerning the interactions that occur between the chaperone and client protein which result in the suppression of aggregation. Approaches such as size exclusion chromatography, electron microscopy, and native mass spectrometry have traditionally been used to examine the end-stage complexes formed between sHsps and client proteins. However, these approaches are limited in their ability to capture the initial binding events between sHsps and client proteins and the dynamic and heterogeneous nature of these complexes. In order to overcome these limitations, we employed a single-molecule fluorescence-based approach that, by utilizing a step-wise photobleaching method, enables the stoichiometries of the chaperone–client complexes in solution to be revealed. In the case of αBc and CLIC1, by monitoring complexes in

solution through time, we have been able to uncover novel details of how this sHsp forms complexes with client proteins.

By using mass photometry, we demonstrated that unlabeled αBc was present as two distinct populations of large (20–40mers) and smaller (<10mers) species at the concentrations used to form complexes with CLIC1 for the analysis by single-molecule fluorescence, consistent with previous studies examining the oligomeric distribution of αBc (8). The mass photometry measurements revealed that addition of the C-terminal cysteine caused little change to the oligomeric distribution of αBc other than a slightly higher proportion of oligomers in the range of 400 to 600 kDa. Incorporation of the fluorescent dye onto this cysteine residue resulted in an increase in the proportion of small αBc oligomers; however, large oligomers still formed in this sample and the protein was still chaperone active. Comparison of the size distribution of αBc obtained *via* mass photometry and the single-molecule fluorescence-based approach indicates that the latter is uniquely able to primarily detect small oligomeric species formed by αBc. This is presumably because these smaller species more readily interact with the coverslip surface used in the single-molecule fluorescence assay, possibly because they have increased amounts of exposed charged and polar residues (15). Moreover, cross-linking of αBc demonstrated that there is also some dissociation of large oligomers as a result of the 1000-fold dilution required for single-molecule fluorescence analysis. In addition, since our single-molecule fluorescence technique is unable to accurately determine the size of αBc oligomers that contain more than 20 subunits, it is limited in its ability to characterize some of the very large oligomers and complexes formed by this sHsp. However, given that the smaller oligomeric species of sHsps have been reported to have enhanced chaperone activity (11–14), proposed to be as a result of increased surface hydrophobicity and dynamism in these dissociated forms (15, 45), our single-molecule fluorescence-based approach is well suited to examining the initial binding events between these small sHsp oligomers and aggregation-prone proteins.

Importantly, the single-molecule methods (mass photometry and single-molecule fluorescence) we have used to describe the oligomeric distribution of αBc involve counting single particles, *i.e.*, a 40-mer oligomer gives the same count (1) as a dimer (1), even though the 40-mer contains 20-times more monomeric subunits. This contrasts to techniques typically used to assess the oligomeric distribution of αBc, such as size-exclusion chromatography (SEC) or analytical ultracentrifugation, which rely on measuring UV absorbance to detect species; thus, using these techniques a single 40-mer gives an absorbance 20-fold higher than a single dimer. This needs to be considered when comparing the relative abundances of protein complexes obtained using these single-molecule techniques with those obtained *via* techniques such as SEC and analytical ultracentrifugation.

Our single-molecule fluorescence data show that the end-stage complexes formed between αBc and CLIC1 are highly heterogeneous, a finding confirmed by TEM analysis of these samples. By examining how these end-stage complexes form, we demonstrate that initially smaller species of αBc (predominantly monomers and dimers) bind to heat-destabilized CLIC1 oligomers. Using this single-molecule approach, we are unable to specifically determine whether there are differences in the binding capacity of small and large oligomers. Nonetheless, our observations validate previous suggestions, based on studying end-stage complexes, that smaller species of sHsps have high chaperone ability and can bind to misfolded proteins (15, 28, 46). Interestingly, we observed that the number of complexes formed between αBc and CLIC1 increased rapidly over the first hour of incubation and reached a plateau after 4 h. During this period, there was an increase in the number of αBc subunits in each αBc–CLIC1 complex. We rationalize this as the recruitment of free αBc subunits onto existing αBc–CLIC1 complexes over time, as has been suggested to occur for other sHsp–client protein interactions (23, 43, 47). Interestingly, we found that prior cross-linking of αBc_{C176} did not significantly impact its capacity to inhibit the heat-induced aggregation of $CLIC1_{C24}$, suggesting that dynamic subunit exchange of αBc oligomers is not required for this chaperone activity and that the additional αBc subunits recruited to existing αBc–CLIC1 complexes do not need to arise as a result of dissociation from larger oligomers.

Varying the molar ratio between CLIC1 and αBc, such that more αBc subunits were available to bind to CLIC1, resulted in an increase in the size of these complexes. We observed a time- and concentration-dependent recruitment of free αBc subunits onto existing αBc–CLIC1 complexes. The lower concentrations of αBc used to form complexes for the single-molecule analyses (2 μM) account for the smaller size of the αBc–CLIC1 complexes detected using this technique compared to the high-molecular-mass complexes observed *via* SEC analysis of samples following the light scattering assay (in which αBc was present at 100 μM). Once formed, cross-linking of the αBc–CLIC1 complexes demonstrates that, upon dilution down to the nM range required for the single-molecule analysis, αBc more readily dissociates from larger sHsp oligomers than from complexes it forms with CLIC1. This is evidenced by our data showing no difference in the size of cross-linked and non-cross-linked αBc–CLIC1 complexes but a decrease in the size of cross-linked and non-cross-linked αBc oligomers. This suggests that the affinity of αBc to destabilized CLIC1 is higher than the affinity of αBc to other αBc subunits. Moreover, this indicates that the observed accumulation of αBc onto αBc–CLIC1 complexes is regulated by the association and dissociation rates of αBc subunits into these complexes and that the dissociation rates from complexes are slower than the timescale of our observations. Hence, αBc subunits are stabilized by the presence of the client protein, a finding supported by the TEM data showing that overall the species formed when αBc is incubated with heat-destabilized CLIC1 are smaller than αBc oligomers. In both prokaryotic (IbpA and IbpB) (47) and eukaryotic sHsp systems (Hsp18.1 and Hsp16.6) (20), sHsp–client complexes are dynamic in that sHsp subunits associate and dissociate from these complexes. Whilst we did not specifically probe for these dynamics in this study, the ability of single-molecule fluorescence techniques to

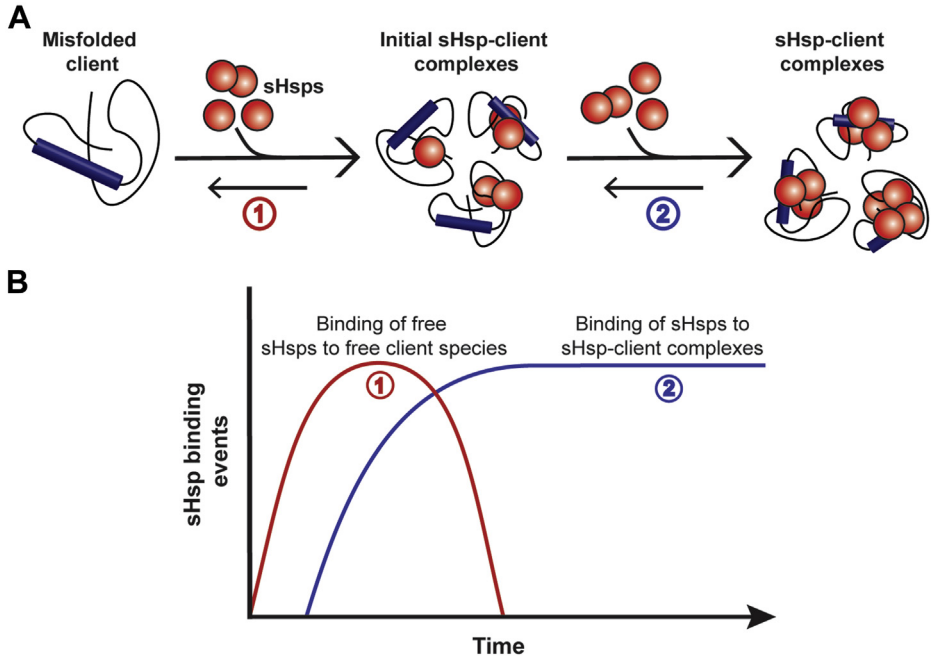

Figure 7. Schematic of two-step mechanism of sHsp–client complex formation. *A*, smaller free sHsps initially recognize and stably bind free misfolded client proteins (1) allowing for subsequent binding of additional free sHsps subunits to form larger sHsp–client complexes (2). *B*, theoretical binding events of sHsp subunits over time showing that initial binding of free sHsps to free clients increases over time (1) until all the misfolded client is bound and additional free sHsp subunits associate with these complexes (2) in order to form larger sHsp–client complexes. sHsp, small heat shock protein.

observe dynamic and transient interactions in real time provides the potential to further develop the approaches we have described here in order to examine if dynamic sHsp subunit exchange occurs on sHsp–client protein complexes.

The binding of monomeric αBc to monomers of CLIC1 did not greatly affect the I_s values, suggesting that the photophysical properties of the dye, such as quantum yield, are largely unaffected by the formation of complexes. However, we did observe that oligomers of αBc and CLIC1 in complex displayed a broader distribution of I_s values, suggesting modest effects of the increased heterogeneity and size of the complex on dye intensity. Therefore, whilst we do observe a small proportion of larger αBc–CLIC1 complexes following incubation, these complexes may be under-represented in our data owing to the variability in the emission intensity of the fluorophores attached to αBc or CLIC1 within these larger complexes. Furthermore, these complexes may also be under-represented in our data owing to the His-tag of the CLIC1, which is required for immobilization, possibly becoming buried during the aggregation and/or binding of multiple αBc subunits.

Taken together, our findings provide direct experimental evidence for a two-step mechanism of sHsp–client complex formation that is in accordance with current models of sHsp chaperone action (Fig. 7) (23, 48–50). First, small sHsp species recognize and stably bind to misfolded client proteins and then these complexes grow through the subsequent addition of additional sHsp subunits onto the newly formed complexes until such a time that the system reaches equilibrium between bound and unbound sHsps and no further growth of the complexes occurs. Thus, the sHsp–client protein complexes we have characterized here are the building blocks of the high-molecular-mass complexes observed using other techniques (such as SEC) in which the sHsp is typically present at higher concentrations than we have used in the single-molecule fluorescence assay. Other than the concentration of the sHsp, the rate of association and dissociation of sHsp subunits from client complexes determines their maximum size. The actual size and the ratio of the sHsp–client protein complexes that are formed may vary for different client proteins. In the cellular context, factors that act to increase the rate of subunit exchange—*e.g.*, phosphorylation (13) or sHsp levels (*e.g.*, as occurs under conditions of cellular stress)—facilitate an increase in chaperone capacity through the provision of increased levels of "active" sHsps. At any given time, the optimum cellular level of sHsps occurs when the amount of the chaperone active species is sufficient to ensure that misfolded clients are stabilized in sHsp–client complexes. The potential for the formation of mixed sHsp hetero-oligomers places another level of complexity and control on sHsp chaperone action in cells.

A two-step mechanism of chaperone action is consistent with data obtained for plant sHsps (23) and the interaction of human αA-crystallin (HSPB4) with client proteins (51). Therefore, this is likely to be a universal functional mechanism of sHsps chaperone action. Future studies employing similar single-molecule fluorescence-based approaches to study the chaperone action of other polydisperse sHsps, such as Hsp27, will provide further insight into if this is indeed the case. Furthermore, similar studies that employ different client proteins would reveal whether the model of sHsp function described in this work is a general mechanism of sHsp–client

interactions. Determining the precise molecular mechanisms of sHsps action is crucial to understanding how these molecular chaperones function to protect the cell from protein misfolding and their overall role in the cellular proteostasis network.

Experimental procedures

Materials, protein expression, and purification

All materials in this work were purchased from Sigma-Aldrich (St Louis, MO, USA) or Amresco (Solon, OH, USA) unless otherwise stated. The pET28a bacterial expression vector, containing human αBc wild-type (αBc_{WT}) or mutant αBc_{C176}, was used for expression of the recombinant proteins (Genscript, Piscataway, NJ). The mutant αBc_{C176} was engineered to contain an additional cysteine (compared with αBc_{WT}) at the extreme C terminus to facilitate the site-specific covalent attachment of a fluorescent dye. Plasmids were transformed into competent *Escherichia coli* (*E. coli*) BL21 (DE3) cells. The αBc variants were purified as described previously (52) and stored at −20 °C.

$CLIC1_{C24}$ in the pET24a vector was produced *via* site-directed mutagenesis of the wild-type genes (Genscript, Piscataway, NJ). The $CLIC1_{C24}$ construct used in this study contained a mutation of one of the native tryptophan residues to phenylalanine (W23F) and mutations of five of the native cysteines to alanines (C59A, C89A, C178A, C191A, and C223A); the remaining cysteine (C24) was not modified so it could be exploited for site-specific fluorescent labeling. $CLIC1_{cysL}$ in the pET24a vector was a kind gift from Dr Sophie Goodchild (Macquarie University, Australia). The $CLIC1_{cysL}$ construct contained mutations of four of the native cysteins to alanines (C89A, C178A, C191A, and C223A); the remaining two cysteins (C24 and C59) were not modified. The pET24a vectors containing the CLIC1 variants ($CLIC1_{C24}$ or $CLIC1_{cysL}$) were each transformed into *E. coli* BL21 CodonPlus (DE3) RIPL cells, and recombinant protein expression was induced by the addition of 0.1 mM IPTG and overnight incubation at 18 °C. The cells were then harvested by centrifugation at 5000*g* for 10 min at 4 °C and the pellet stored at −20 °C. Cells were resuspended in 50 mM Tris-base (pH 8.0) containing 100 mM NaCl, 0.5 mg/ml lysozyme, and EDTA-free cocktail protease inhibitor, incubated for 20 min at 4 °C and then sonicated to further lyse cells and shear DNA. The cell lysate was then clarified by centrifugation twice at 24,000*g* for 20 min, passed through a 0.45-μM filter, and applied to a 5-ml HisTrap Sephadex column (GE Healthcare, USA) equilibrated in 50 mM Tris-base (pH 8.0) containing 5 mM imidazole and 300 mM NaCl. The bound recombinant protein was then eluted with 500 mM imidazole and loaded onto an s75 Superdex size-exclusion column equilibrated in 50 mM phosphate buffer (pH 7.4). The recombinant protein was concentrated, snap-frozen in liquid nitrogen, and stored at −20 °C until use. The SOD1 used in this work was a gift from Prof. Justin Yerbury (University of Wollongong, Australia).

In vitro *amorphous aggregation assays*

In vitro aggregation assays were performed to assess the ability of αBc_{WT} and αBc_{C176} to inhibit the amorphous aggregation of $CLIC1_{cysL}$ or $CLIC1_{C24}$. CLIC1 (either 50 μM for $CLIC1_{cysL}$ or 30 μM for the more destabilized $CLIC1_{C24}$ isoform) was incubated in 50 mM phosphate buffer (pH 7.4) supplemented with 10 mM DTT in the presence or absence of varying molar ratios of αBc (between 1:0.5 and 1:64, α Bc:CLIC1). CLIC1 incubated in the presence of SOD1 or ovalbumin at a 1:0.5 molar ratio (SOD1/Ova:CLIC1) acted as a control for the chaperone-specific inhibition of CLIC1 aggregation. Samples were prepared in duplicate in a Greiner Bio-One 384-well microplate (Greiner Bio-One, Freickenhausen, Germany) and sealed to prevent evaporation. The aggregation of CLIC1 was monitored by measuring the light scatter at 340 nm using a FLUOstar Optima plate reader at 37 °C for 20 h. To quantify the ability of the αBc variants to prevent CLIC1 aggregation, the percent inhibition of aggregation was calculated using the formula: % inhibition = $((\Delta Ic - \Delta Is)/\Delta Ic) \times 100$, where ΔIc and ΔIs are the change in absorbance in the absence and presence of chaperone at the end of the assay, respectively. The percent inhibition of aggregation afforded by the αBc variants is reported as the mean ± SD of three independent experiments.

Analytical SEC and SDS-PAGE

Further characterization of the interaction between $CLIC1_{cysL}$ and αBc_{WT} was achieved by analyzing samples by SEC at the end of the aggregation assays. Samples containing $CLIC1_{cysL}$ (50 μM) in the presence or absence of αBc_{WT} (100 μM) were collected immediately following incubation and centrifuged at 20,000*g* for 10 min to remove any insoluble protein. Supernatants were then collected and loaded (80 μl) onto a Superdex 200 HR 10/300 GL column (GE Healthcare, UK) pre-equilibrated in 50 mM phosphate buffer (pH 7.4) and calibrated using Bio-Rad gel filtration standards (USA). Samples were eluted at 0.5 ml/min, and an in-line UV detector was used to monitor the elution of proteins from the column *via* their absorbance at 280 nm. Fractions corresponding to peaks on the chromatogram were collected and mixed with an equal volume of reducing sample buffer such that the final concentration of 2-mercaptethanol was 2.5% (v/v). These samples were subsequently heated at 95 °C before being run on a 12% (v/v) acrylamide gel for analysis *via* SDS-PAGE.

Fluorescent labeling of proteins

For smFRET experiments, $CLIC1_{C24}$ was labeled with an Alexa Fluor 555 donor maleimide fluorophore (AF555-$CLIC1_{C24}$), and αBc_{C176} was labeled with an Alexa Fluor 647 maleimide acceptor fluorophore (AF647-αBc_{C176}). For two-color single-molecule experiments, $CLIC1_{C24}$ and αBc_{C176} were labeled with Alexa Fluor 647 and Alexa Fluor 488 maleimide fluorophores, respectively. Proteins were fluorescently labeled as previously described with some modifications (53). Briefly, proteins to be labeled were incubated in 5 mM tris(2-carboxyethyl)phosphine and 70% (w/v) ammonium sulfate powder and placed on a rotator at 4 °C for 1 h. Proteins were then centrifuged, and the pellet was resuspended in degassed buffer A (100 mM Na_2PO_4 (pH 7.4), 200 mM NaCl, 1 mM EDTA, 70% (w/v) ammonium sulfate). The protein was centrifuged, and the washed pellet was resuspended in buffer B

(100 mM Na_2PO_4 (pH 7.4), 200 mM NaCl, 1 mM EDTA) containing a 5-fold molar excess of maleimide-conjugated fluorophore. The protein was then incubated on a rotator at room temperature for 3 h. Following the coupling reaction, excess dye was removed by gel filtration chromatography using a 7 K MWCO Zebra Spin Desalting column equilibrated in 50 mM phosphate buffer (pH 7.4). The concentration and degree of labeling was calculated for AF647-$CLIC1_{C24}$ (96%), AF555-$CLIC1_{C24}$ (82%), AF647-αBc_{C176} (77%), and AF488-αBc_{C176} (>95%) by UV absorbance or denaturing mass spectrometry (Table S1). The proteins were stored at −20 °C until use.

Coverslip preparation and immobilization of samples for smFRET and two-color TIRF microscopy

Microfluidic flow cells were constructed by placing polydimethylsiloxane lids on 24 × 24-mm coverslips that had been PEG-biotin-functionalized (54). Coverslips were functionalized by treatment with 100% ethanol and 5 M KOH, before aminosilanization was carried out in a 1% (v/v) (3-aminopropyl) triethoxysilane (Alfa Aesar, UK) solution. PEGylation of coverslips was performed by incubating coverslips with 1:10 mixture of biotinPEG-SVA and mPEG-SVA (Laysan Bio, AL) prepared in 50 mM 3-(N-morpholino) propanesulfonic acid (pH 7.5) solution for 3 h. Coverslips were further functionalized by an additional PEGylation overnight before being stored under nitrogen gas at −20 °C. Inlets and outlets in the polydimethylsiloxane were prepared using PE-20 tubing (Instech, PA, USA) that allowed washing and addition of samples onto the coverslip surface. Neutravidin (125 μg/ml) was incubated in the flow cell for 10 min and washed with 50 mM phosphate buffer (pH 7.4) supplemented with 6-hydroxy-2,5,7,8-tetramethylchroman-2-carboxylic acid (6 mM, TROLOX) (imaging buffer). To help prevent nonspecific interactions of proteins with the coverslip surface, the microfluidic channel was blocked with 2% (v/v) Tween-20 for 20 min (55) and then washed extensively with imaging buffer. To facilitate immobilization of His-tagged CLIC1 to the coverslip surface, anti-6X His-tag antibody (1 μg/ml) was incubated in the flow cell for 10 min. Finally, preformed CLIC1–αBc complexes were diluted 1:1000, incubated in the flow cell for 10 min, and washed with imaging buffer to remove unbound proteins. To reduce blinking and unavoidable photobleaching of fluorescent dyes during imaging, an oxygen scavenger system (OSS) consisting of protocatechuic acid (2.5 mM) and protocatechuate-3,4-dioxygenase (50 nM) in imaging buffer was introduced into the flow cell prior to image acquisition.

smFRET sample preparation, instrument setup, and data analysis

To confirm that αBc_{C176} formed complexes with aggregating $CLIC1_{C24}$, smFRET experiments were performed. AF555-$CLIC1_{C24}$ (1 μM) was incubated in the presence of AF647-αBc_{C176} (2 μM) for 20 h at 37 °C in 50 mM phosphate buffer (pH 7.4). The sample was then diluted 1:1000 in imaging buffer and immediately loaded into a flow cell for TIRF microscopy. Single-molecule measurements were performed at room temperature (approx. 20 °C) on a custom-built TIRF microscope with a sapphire green (532 nm) laser that has been previously described (56). Images were acquired every 200 msec, and single-molecule fluorescence intensity time trajectories from multiple fields of view (FOVs) were generated and analyzed using a Matlab-based software program (MASH-FRET) (57). Donor leakage into the acceptor channel was corrected during image analysis.

Two-color TIRF microscopy instrument setup and data acquisition

Samples were imaged at room temperature (approx. 20 °C) using a custom-built total internal reflection fluorescence microscope system constructed around an inverted optical microscope (IX70, Olympus, Tokyo, Japan). Samples were illuminated simultaneously by a solid-state 488-nm laser (0.75 W/cm^2; 150 mW Sapphire 488 nm, Coherent, Santa Clara, CA, USA) and 637-nm laser (6.5 W/cm^2; 140 mW Vortran, Sacramento, CA, USA), which were aligned and directed off a dichroic mirror (Di01-R405/488/561/635, Semrock, Rochester, NY, USA) to the back aperture of a 1.49 NA TIRF objective lens (100 x UApoN model, Olympus) mounted on the optical microscope. Fluorescence emission was collected by the same objective, and the returning TIRF beam was filtered by a dichroic mirror (Di01-R405/488/561/635, Semrock). Then, incoming emission signals were separated using a dual view of 635-nm cutoff dichroic filter (Photometric DV2) that split incoming emission signals into two and directed them to a charge-coupled device chip, allowing simultaneous imaging of two colors on each half of the same chip, and passed through appropriate band-pass filters (BLP01–488R for AF488 and BLP01–633R for AF647) onto a EM-CCD camera (ImageEM, Hamamatsu, Japan). Control of the hardware was performed using the microscopy platform Micromanager (NIH, USA), and the camera was in frame transfer mode at 5 Hz. Multiple single-molecule movies of each sample were recorded at different FOVs, with images taken every 200 msec. All excitation intensities were kept constant for all samples imaged.

Single-molecule characterization of surface binding of heated $CLIC1_{C24}$

To investigate the ability of heated fluorescently labeled $CLIC1_{C24}$ to bind surface immobilized anti-His antibodies, AF647-$CLIC_{C24}$ (1 μM) was incubated at 37 °C for 2 h in 50 mM phosphate buffer (pH 7.4). The sample was subsequently diluted 1:1000 into imaging buffer and immediately loaded into flow cells that had been incubated in the presence or absence of the anti-6X His-tag antibody (1 μg/ml). Following a 10-min incubation, the flow cells were washed with imaging buffer containing an OSS to remove unbound proteins and immediately imaged with the red (637 nm) laser. The number of foci per FOV and the fluorescent intensity of each focus were calculated. The number of foci per FOV for each treatment group is reported as the mean ± standard

deviation (n = 12). The fluorescent intensity of $CLIC1_{C24}$ species in the treatment groups are presented as violin plots showing the kernel probability distribution, median, and interquartile range.

In order to examine the binding efficiencies of folded and thermally destabilized $CLIC1_{C24}$, AF555-labeled $CLIC1_{C24}$ (1 μM) was incubated at 37 °C (heated) for 2 h in 50 mM phosphate buffer (pH 7.4). AF647-labeled $CLIC1_{C24}$ (1 μM) was incubated with heated or nonheated AF555-$CLIC1_{C24}$ (1 μM) in 50 mM phosphate buffer (pH 7.4) on ice for 5 min. Samples were diluted 1:1000 in imaging buffer and immediately loaded into flow cells constructed with functionalized coverslips containing a surface-immobilized anti-6X His-tag antibody. Samples were incubated for 10 min before being washed with imaging buffer containing an OSS. Samples were imaged with a red (637 nm) laser until all visible foci were photobleached followed by a green (532 nm) laser to prevent the chances of any FRET occurring between the two fluorescently labeled $CLIC1_{C24}$ species. The number of AF647-$CLIC1_{C24}$ and AF555-$CLIC1_{C24}$ foci in each image was counted and corrected to account for differences in the labeling efficiencies of AF647-$CLIC1_{C24}$ (86%) and AF555-$CLIC1_{C24}$ (73%). These values were then used to calculate the relative abundance of each fluorescently labeled $CLIC1_{C24}$ per FOV.

Single-molecule two-color sample preparation

Two-color TIRF microscopy was used to characterize the complexes formed between αBc and CLIC1. To determine how the stoichiometries of αBc–CLIC1 complexes changed over time, 1 μM Alexa Fluor 647-labeled $CLIC1_{C24}$ (AF647-$CLIC1_{C24}$) was incubated in 50 mM phosphate buffer (pH 7.4) at 37 °C for 10 h in the presence of 2 μM Alexa Fluor 488-labeled αBc_{C176} (AF488-αBc_{C176}). Aliquots were taken from the reaction at 0, 0.25, 0.5, 0.75, 1, 4, 8, and 10 h for single-molecule imaging. To examine the effect of chaperone concentration on the stoichiometries of αBc–CLIC1 complexes, AF647-$CLIC1_{C24}$ (1 μM) was incubated under the same conditions as described above except in the presence of varying molar ratios of AF488-αBc_{C176} (0.25:1, 0.5:1, 1:1, 2:1, and 4:1 [αBc:CLIC1]) for 8 h. All samples were diluted 1:1000 into imaging buffer and immediately loaded into flow cells for imaging.

Two-color total internal reflection fluorescence microscopy data and statistical analysis

Images were corrected for electronic offset and inhomogeneity of the excitation beam laser before intensity time trajectories were generated for all fluorescent molecules using custom-written scripts in Fiji (58). The initial fluorescence intensity (I_0) was calculated by averaging the first 20 intensity values for all fluorescent proteins identified. Fluorescent trajectories of molecules with distinct photobleaching events for AF647-$CLIC1_{C24}$ and AF488-αBc_{C176} were manually identified and were fit by change-point analysis (59, 60) to determine the fluorescence intensity of each single-photobleaching event (I_s). These I_s values were then collectively fit to a Gaussian distribution from which the mean intensity of a single photobleaching event ($I_{s\text{-}mean}$) was calculated. The $I_{s\text{-}mean}$ values were then used to calculate the number of *FPP* using the equation $FPP = I_0/I_{s\text{-}mean}$. At each treatment point (timepoint or concentration), *FPP* for AF647-$CLIC1_{C24}$ or AF488-αBc_{C176} were combined to determine oligomer size distributions. Herein oligomer size refers to the number of subunits of a given protein in an oligomer (*e.g.*, for a single complex that contains 5 AF647-$CLIC1_{C24}$ subunits, the $CLIC1_{C24}$ oligomer size for that complex is 5). These oligomer sizes are presented as violin plots showing the kernel probability distribution, median, and interquartile range for each treatment. As fluorophores can self-quench when present at high local concentrations, complexes that contained more than 20 subunits of $CLIC1_{C24}$ or αBc_{C176} were excluded from this detailed analysis of subunit architecture. Importantly, the maximum proportion of species present in solution that could not be characterized in detail was 12%; this was for the sample containing αBc_{C176} and $CLIC1_{C24}$ incubated for 10 h at 37 °C at a molar ratio of 2:1 (αBc_{C176}–$CLIC1_{C24}$) (Fig. S10*A*).

All plots were generated, and statistical analysis was performed, using Prism8 (GraphPad, CA, USA). Data were analyzed *via* student's *t* test or an ANOVA with subsequent Kruskal–Wallis tests followed by Dunn's multiple comparisons (*p* values are given, whereby a *p* value of less than 0.05 was considered statistically significant). Stoichiometries of complexes were calculated by pairing of colocalized *FPP* for AF647-$CLIC1_{C24}$ and AF488-αBc_{C176}. Heatmaps were generated in MATLAB using home-written scripts.

Data availability

All data and source code used in this work are available on request from the authors.

Supporting information—This article contains supporting information (61).

Acknowledgments—We thank Drs Philipp Kukura and Weston Struwe (University of Oxford, UK) for their help with the mass photometry. We also thank Dr Sophie Goodchild (Macquarie University, Australia) and Prof Paul Curmi (The University of NSW, Australia) for their help and guidance with the design of the CLIC1 mutant proteins used in this work. We thank Dr James Bouwer (UOW Cryo-electron microscopy facility) for help with TEM imaging. Finally, we thank staff in Molecular Horizons and the Illawarra Heath and Medical Research Institute for technical and administrative support.

Author contributions—C. L. J., B. P. P., H. E., and A. M. v. O. formulated the experimental approach. N. R. M. made the recombinant CLIC1 and performed *in vitro* aggregation assays and size exclusion chromatography. C. L. J., N. R. M., and B. P. P. developed the conditions for the single-molecule approach used in this work. G. W. and J. L. P. B. performed mass photometry experiments. C. L. J. performed all other experiments, analyzed the data,

constructed the figures, and wrote the initial manuscript. C. L. J., N. R. M., B. P. P., J. L. P. B., H. E., and A. M. v. O. edited the manuscript and approved the submission of the final manuscript.

Funding and additional information—This research performed by C. L. J. and N. R. M. has been conducted with the support of the Australian Government Research Training Program Scholarship. A. M. v. O. is supported by an ARC Laureate Fellowship (FL140100027).

Conflict of interest—The authors declare that they have no conflicts of interest with the contents of this article.

Abbreviations—The abbreviations used are: αBc, αB-crystallin; CLIC1, chloride intracellular channel 1; FPP, fluorescently-labeled proteins per point; GST, glutathione-S-transferase; I_0, initial fluorescence intensity; I_s, fluorescent intensity of each single-photobleaching event; $I_{s\text{-}mean}$, mean intensity of a single photobleaching event; OSS, oxygen scavenger system; proteostasis, protein homeostasis; smFRET, single-molecule FRET; SOD1, superoxide dismutase 1; sHsp, small heat shock protein; TIRF, total internal reflection fluorescence.

References

1. Jakob, U., Gaestel, M., Engel, K., and Buchner, J. (1993) Small heat shock proteins are molecular chaperones. *J. Biol. Chem.* **268**, 1517–1520
2. Horwitz, J. (1992) Alpha-crystallin can function as a molecular chaperone. *Proc. Natl. Acad. Sci. U. S. A.* **89**, 10449–10453
3. de Jong, W. W., Leunissen, J. A., and Voorter, C. (1993) Evolution of the alpha-crystallin/small heat-shock protein family. *Mol. Biol. Evol.* **10**, 103–126
4. Clark, J. I., and Muchowski, P. J. (2000) Small heat-shock proteins and their potential role in human disease. *Curr. Opin. Struct. Biol.* **10**, 52–59
5. Ciocca, D. R., and Calderwood, S. K. (2005) Heat shock proteins in cancer: diagnostic, prognostic, predictive, and treatment implications. *Cell Stress Chaperones* **10**, 86
6. Sun, Y., and MacRae, T. H. (2005) The small heat shock proteins and their role in human disease. *FEBS J.* **272**, 2613–2627
7. Basha, E., O'Neill, H., and Vierling, E. (2012) Small heat shock proteins and α-crystallins: dynamic proteins with flexible functions. *Trends Biochem. Sci.* **37**, 106–117
8. Aquilina, J. A., Benesch, J. L. P., Bateman, O. A., Slingsby, C., and Robinson, C. V. (2003) Polydispersity of a mammalian chaperone: mass spectrometry reveals the population of oligomers in αB-crystallin. *Proc. Natl. Acad. Sci. U. S. A.* **100**, 10611–10616
9. Baldwin, A. J., Lioe, H., Robinson, C. V., Kay, L. E., and Benesch, J. L. (2011) αB-crystallin polydispersity is a consequence of unbiased quaternary dynamics. *J. Mol. Biol.* **413**, 297–309
10. Haslbeck, M., Weinkauf, S., and Buchner, J. (2015) Regulation of the chaperone function of small Hsps. In *The Big Book on Small Heat Shock Proteins*, Springer International Publishing, Switzerland: 155–178
11. Jovcevski, B., Kelly, M. A., Rote, A. P., Berg, T., Gastall, H. Y., Benesch, J. L. P., Aquilina, J. A., and Ecroyd, H. (2015) Phosphomimics destabilize Hsp27 oligomeric assemblies and enhance chaperone activity. *Chem. Biol.* **22**, 186–195
12. Hayes, D., Napoli, V., Mazurkie, A., Stafford, W. F., and Graceffa, P. (2009) Phosphorylation dependence of hsp27 multimeric size and molecular chaperone function. *J. Biol. Chem.* **284**, 18801–18807
13. Peschek, J., Braun, N., Rohrberg, J., Back, K. C., Kriehuber, T., Kastenmüller, A., Weinkauf, S., and Buchner, J. (2013) Regulated structural transitions unleash the chaperone activity of αB-crystallin. *Proc. Natl. Acad. Sci. U. S. A.* **110**, E3780–E3789
14. Ecroyd, H., Meehan, S., Horwitz, J., Aquilina, J. A., Benesch, J. L., Robinson, C. V., Macphee, C. E., and Carver, J. A. (2006) Mimicking phosphorylation of αB-crystallin affects its chaperone activity. *Biochem. J.* **401**, 129–141
15. Alderson, T. R., Roche, J., Gastall, H. Y., Dias, D. M., Pritišanac, I., Ying, J., Bax, A., Benesch, J. L., and Baldwin, A. J. (2019) Local unfolding of the HSP27 monomer regulates chaperone activity. *Nat. Commun.* **10**, 1068
16. Lindner, R. A., Kapur, A., and Carver, J. A. (1997) The interaction of the molecular chaperone, α-crystallin, with molten globule states of bovine α-lactalbumin. *J. Biol. Chem.* **272**, 27722–27729
17. Regini, J. W., Ecroyd, H., Meehan, S., Bremmell, K., Clarke, M. J., Lammie, D., Wess, T., and Carver, J. A. (2010) The interaction of unfolding α-lactalbumin and malate dehydrogenase with the molecular chaperone αB-crystallin: a light and X-ray scattering investigation. *Mol. Vis.* **16**, 2446–2456
18. Stromer, T., Ehrnsperger, M., Gaestel, M., and Buchner, J. (2003) Analysis of the interaction of small heat shock proteins with unfolding proteins. *J. Biol. Chem.* **278**, 18015–18021
19. Basha, E., Lee, G. J., Demeler, B., and Vierling, E. (2004) Chaperone activity of cytosolic small heat shock proteins from wheat. *Eur. J. Biochem.* **271**, 1426–1436
20. Friedrich, K. L., Giese, K. C., Buan, N. R., and Vierling, E. (2004) Interactions between small heat shock protein subunits and substrate in small heat shock protein-substrate complexes. *J. Biol. Chem.* **279**, 1080–1089
21. Lee, G. J., Roseman, A. M., Saibil, H. R., and Vierling, E. (1997) A small heat shock protein stably binds heat-denatured model substrates and can maintain a substrate in a folding-competent state. *EMBO J.* **16**, 659–671
22. Stengel, F., Baldwin, A. J., Bush, M. F., Hilton, G. R., Lioe, H., Basha, E., Jaya, N., Vierling, E., and Benesch, J. L. (2012) Dissecting heterogeneous molecular chaperone complexes using a mass spectrum deconvolution approach. *Chem. Biol.* **19**, 599–607
23. Stengel, F., Baldwin, A. J., Painter, A. J., Jaya, N., Basha, E., Kay, L. E., Vierling, E., Robinson, C. V., and Benesch, J. L. P. (2010) Quaternary dynamics and plasticity underlie small heat shock protein chaperone function. *Proc. Natl. Acad. Sci. U. S. A.* **107**, 2007–2012
24. van Montfort, R. L., Basha, E., Friedrich, K. L., Slingsby, C., and Vierling, E. (2001) Crystal structure and assembly of a eukaryotic small heat shock protein. *Nat. Struct. Biol.* **8**, 1025–1030
25. Giese, K. C., and Vierling, E. (2002) Changes in oligomerization are essential for the chaperone activity of a small heat shock protein *in vivo* and *in vitro*. *J. Biol. Chem.* **277**, 46310–46318
26. Shashidharamurthy, R., Koteiche, H. A., Dong, J., and McHaourab, H. S. (2005) Mechanism of chaperone function in small heat shock proteins: dissociation of the HSP27 oligomer is required for recognition and binding of destabilized T4 lysozyme. *J. Biol. Chem.* **280**, 5281–5289
27. McHaourab, H. S., Godar, J. A., and Stewart, P. L. (2009) Structure and mechanism of protein stability sensors: chaperone activity of small heat shock proteins. *Biochemistry* **48**, 3828–3837
28. Santhanagopalan, I., Degiacomi, M. T., Shepherd, D. A., Hochberg, G. K., Benesch, J. L., and Vierling, E. (2018) It takes a dimer to tango: oligomeric small heat shock proteins dissociate to capture substrate. *J. Biol. Chem.* **293**, 19511–19521
29. Johnston, C. L., Marzano, N. R., van Oijen, A. M., and Ecroyd, H. (2018) Using single-molecule approaches to understand the molecular mechanisms of heat-shock protein chaperone function. *J. Mol. Biol.* **430**, 4525–4546
30. Avellaneda, M. J., Koers, E. J., Naqvi, M. M., and Tans, S. J. (2017) The chaperone toolbox at the single-molecule level: from clamping to confining. *Protein Sci.* **26**, 1291–1302
31. Littler, D. R., Harrop, S. J., Goodchild, S. C., Phang, J. M., Mynott, A. V., Jiang, L., Valenzuela, S. M., Mazzanti, M., Brown, L. J., and Breit, S. N. (2010) The enigma of the CLIC proteins: ion channels, redox proteins, enzymes, scaffolding proteins? *FEBS Lett.* **584**, 2093–2101
32. Harrop, S. J., DeMaere, M. Z., Fairlie, W. D., Reztsova, T., Valenzuela, S. M., Mazzanti, M., Tonini, R., Qiu, M. R., Jankova, L., and Warton, K. (2001) Crystal structure of a soluble form of the intracellular chloride ion channel CLIC1 (NCC27) at 1.4-Å resolution. *J. Biol. Chem.* **276**, 44993–45000
33. Berry, K. L., and Hobert, O. (2006) Mapping functional domains of chloride intracellular channel (CLIC) proteins *in vivo*. *J. Mol. Biol.* **359**, 1316–1333

34. McLoughlin, F., Basha, E., Fowler, M. E., Kim, M., Bordowitz, J., Katiyar-Agarwal, S., and Vierling, E. J. P. P. (2016) Class I and II small heat shock proteins together with HSP101 protect protein translation factors during heat stress. *Plant Physiol.* **172**, 1221–1236
35. Préville, X., Salvemini, F., Giraud, S., Chaufour, S., Paul, C., Stepien, G., Ursini, M. V., and Arrigo, A. P. (1999) Mammalian small stress proteins protect against oxidative stress through their ability to increase glucose-6-phosphate dehydrogenase activity and by maintaining optimal cellular detoxifying machinery. *Exp. Cell Res.* **247**, 61–78
36. Fanucchi, S., Adamson, R. J., and Dirr, H. W. (2008) Formation of an unfolding intermediate state of soluble chloride intracellular channel protein CLIC1 at acidic pH. *Biochemistry* **47**, 11674–11681
37. Cross, M., Fernandes, M., Dirr, H., and Fanucchi, S. (2015) Glutamate 85 and glutamate 228 contribute to the pH-response of the soluble form of chloride intracellular channel 1. *Mol. Cell Biochem.* **398**, 83–93
38. Haslbeck, M., and Vierling, E. (2015) A first line of stress defense: small heat shock proteins and their function in protein homeostasis. *J. Mol. Biol.* **427**, 1537–1548
39. Goodchild, S. C., Angstmann, C. N., Breit, S. N., Curmi, P. M., and Brown, L. J. (2011) Transmembrane extension and oligomerization of the CLIC1 chloride intracellular channel protein upon membrane interaction. *Biochemistry* **50**, 10887–10897
40. Mymrikov, E. V., Daake, M., Richter, B., Haslbeck, M., and Buchner, J. (2017) The chaperone activity and substrate spectrum of human small heat shock proteins. *J. Biol. Chem.* **292**, 672–684
41. Fu, X. (2014) Chaperone function and mechanism of small heat-shock proteins. *Acta Biochim. Biophys. Sin.* **46**, 347–356
42. Mogk, A., Schlieker, C., Friedrich, K. L., Schönfeld, H.-J., Vierling, E., and Bukau, B. (2003) Refolding of substrates bound to small Hsps relies on a disaggregation reaction mediated most efficiently by ClpB/DnaK. *J. Biol. Chem.* **278**, 31033–31042
43. Haslbeck, M., Walke, S., Stromer, T., Ehrnsperger, M., White, H. E., Chen, S., Saibil, H. R., and Buchner, J. (1999) Hsp26: a temperature-regulated chaperone. *EMBO J.* **18**, 6744–6751
44. Gade Malmos, K., Blancas-Mejia, L. M., Weber, B., Buchner, J., Ramirez-Alvarado, M., Naiki, H., and Otzen, D. (2017) ThT 101: a primer on the use of thioflavin T to investigate amyloid formation. *Amyloid* **24**, 1–16
45. Hayashi, J., and Carver, J. A. (2020) The multifaceted nature of αB-crystallin. *Cell Stress Chaperones* **25**, 639–654
46. Hochberg, G. K., Ecroyd, H., Liu, C., Cox, D., Cascio, D., Sawaya, M. R., Collier, M. P., Stroud, J., Carver, J. A., and Baldwin, A. J. (2014) The structured core domain of αB-crystallin can prevent amyloid fibrillation and associated toxicity. *Proc. Natl. Acad. Sci. U. S. A.* **111**, E1562–E1570
47. Żwirowski, S., Kłosowska, A., Obuchowski, I., Nillegoda, N. B., Piróg, A., Ziętkiewicz, S., Bukau, B., Mogk, A., and Liberek, K. (2017) Hsp70 displaces small heat shock proteins from aggregates to initiate protein refolding. *EMBO J.* **36**, 783–796
48. Treweek, T. M., Meehan, S., Ecroyd, H., and Carver, J. A. (2015) Small heat-shock proteins: important players in regulating cellular proteostasis. *Cell Mol. Life Sci.* **72**, 429–451
49. Mogk, A., Ruger-Herreros, C., and Bukau, B. (2019) Cellular functions and mechanisms of action of small heat shock proteins. *Annu. Rev. Microbiol.* **73**, 89–110
50. Haslbeck, M., Weinkauf, S., and Buchner, J. (2019) Small heat shock proteins: simplicity meets complexity. *J. Biol. Chem.* **294**, 2121–2132
51. McHaourab, H. S., Dodson, E. K., and Koteiche, H. A. (2002) Mechanism of chaperone function in small heat shock proteins. Two-mode binding of the excited states of T4 lysozyme mutants by alphaA-crystallin. *J. Biol. Chem.* **277**, 40557
52. Horwitz, J., Huang, Q.-L., LINLIN, D., and Bova, M. P. (1998) Lens alpha-crystallin: chaperone-like properties. *Methods Enzymol.* **290**, 365–383
53. Kim, Y., Ho, S. O., Gassman, N. R., Korlann, Y., Landorf, E. V., Collart, F. R., and Weiss, S. (2008) Efficient site-specific labeling of proteins via cysteines. *Bioconjug. Chem.* **19**, 786–791
54. Chandradoss, S. D., Haagsma, A. C., Lee, Y. K., Hwang, J.-H., Nam, J.-M., and Joo, C. J. J. (2014) Surface passivation for single-molecule protein studies. *J. Vis. Exp.* **86**, e50549
55. Pan, H., Xia, Y., Qin, M., Cao, Y., and Wang, W. (2015) A simple procedure to improve the surface passivation for single molecule fluorescence studies. *Phys. Biol.* **12**, 045006
56. Zhong, Y., Paudel, B. P., Ryan, D. P., Low, J. K., Franck, C., Patel, K., Bedward, M. J., Torrado, M., Payne, R. J., and van Oijen, A. M. (2020) CHD4 slides nucleosomes by decoupling entry-and exit-side DNA translocation. *Nat. Commun.* **11**, 1–14
57. Hadzic, M. C., Kowerko, D., Börner, R., Zelger-Paulus, S., and Sigel, R. K. (2016) *Detailed Analysis of Complex Single Molecule FRET Data with the Software MASH*, SPIE, International Society for Optics and Photonics, San Francisco, CA
58. Schindelin, J., Arganda-Carreras, I., Frise, E., Kaynig, V., Longair, M., Pietzsch, T., Preibisch, S., Rueden, C., Saalfeld, S., and Schmid, B. (2012) Fiji: an open-source platform for biological-image analysis. *Nat. Methods* **9**, 676–682
59. Duderstadt, K. E., Geertsema, H. J., Stratmann, S. A., Punter, C. M., Kulczyk, A. W., Richardson, C. C., and van Oijen, A. M. J. M. C. (2016) Simultaneous real-time imaging of leading and lagging strand synthesis reveals the coordination dynamics of single replisomes. *Mol. Cell* **64**, 1035–1047
60. Watkins, L. P., and Yang, H. J. (2005) Detection of intensity change points in time-resolved single-molecule measurements. *J. Phys. Chem.* **109**, 617–628
61. Young, G., Hundt, N., Cole, D., Fineberg, A., Andrecka, J., Tyler, A., Olerinyova, A., Ansari, A., Marklund, E. G., and Collier, M. P. (2018) Quantitative mass imaging of single biological macromolecules. *Science* **360**, 423–427